Neutral boron-interstitial clusters in crystalline silicon

Paola Alippi*
CNR-IMM, Sezione Catania, Stradale Primosole 50, 95121 Catania, Italy

P. Ruggerone and L. Colombo
INFM-SLACS and Department of Physics, University of Cagliari, Cittadella Universitaria, I-09042 Monserrato (CA), Italy
(Received 21 May 2003; revised manuscript received 28 October 2003; published 10 March 2004)

The formation of B clusters inside ultrashallow junctions is one of limiting factors in the miniaturization process of electronic devices. The assembling of these clusters corresponds to a reduction of the electrical activity of the doping process. Exploiting hierarchically different simulation techniques, we investigate structural and electronic properties of small B clusters inside a crystalline Si matrix. Density-functional–theory-tight-binding molecular dynamics simulations are carried out as scouts selecting the candidates to be analyzed in depth via *ab initio* calculations. The latter provide insights into the electronic properties of the B clusters, identifying the fingerprints of interstitialcy and chemical composition in their densities of states.

DOI: 10.1103/PhysRevB.69.125205 PACS number(s): 71.55.−i, 66.30.Jt, 71.15.Mb

I. INTRODUCTION

Boron is the most widely used *p*-type dopant of silicon in modern electronic devices. As technology generations advance and devices reduce in size, it is necessary to create, by means of ion-implantation and rapid thermal annealing process, sharp, ultrashallow profiles with high concentrations of electrically active B. However, two related processes, associated with the implantation and the annealing, limit the achievement of this goal. These are the transient enhanced diffusion of B atoms during high-temperature annealing when a large concentration of intrinsic defects is present[1] and the existence of electrically inactive, multiatom B-Si defect complexes, resulting form the strong dopant supersaturation during the implant process. In particular, secondary ion-mass spectroscopies (SIMS) and electrical measurements[2] in B-doped silicon samples have shown that B precipitates form at concentrations much lower than the equilibrium solid solubility, with detrimental effects for device properties.

The prediction of B distribution under implant conditions needs an accurate and efficient modeling of the B-Si clustering process. This has fostered several theoretical works in the past few years. The study of Pelaz and co-workers[3] was based on kinetic Monte Carlo simulations of experimental SIMS profiles. They proposed that an interstitial-rich path is efficient in the early stages of the implant, while dissolution of clusters should happen through the subsequent much slower release of Si-interstitial atoms. The Monte Carlo simulations have to rely on a set of values for clusters energetics, and those used by Pelaz *et al.*[3] ranged from semi-empirical to *ab initio*, and even experimental data are included in this set. Such heterogeneous variety of supporting data makes their analysis questionable as far reliability.

More recent first-principles calculations[4,5] have presented the structures and energetics of boron-interstitial clusters (from here on denoted as B_nI_m) resulting from total energy minimizations. They found the B_3I_1 cluster in its -1 charge state to be remarkably stable, acting thus as seed of nucleation for further growth. The energy rank proposed by both research groups clearly ruled out the occurrence of pure substitutional B clusters, indicating the presence of interstitial species as stability requirement for the assembled structures. Albeit concentrated on the clustering process of B in Si crystals, a third *ab initio* work[6] confirmed the structural results obtained by Lenosky *et al.*[5] and by Liu *et al.*[4] Despite the very careful and thorough analysis covering structures and dynamics and despite the technological importance of the issue, an analogous detailed investigation on the electronic properties of the B clusters is not present in the literature. Our work is intended as a contribution to this still unexplored topic. An accurate identification of possible extrinsic electronic levels is the starting point for characterizing the response of the aggregates to electrical driving. Furthermore, experimentally there is no direct way to detect the structures of many B clusters because of their limited sizes. Therefore, the comparison between the calculated electronic structures associated to a given aggregate and the measured features related to deep levels yields an additional tool for pinpointing the structures present in the investigated sample.

It is clear that these problems are strongly heterogeneous as to the level of accuracy required and the size of the systems to be simulated, and no single theoretical technique can face them all with the same effectiveness. The presence of several B atoms and interstitial species forming aggregates raises the number of degrees of freedom in the investigated system, increasing the dimension of the configuration space to be investigated. Thus, we apply a hierarchy of different complementary methodologies to the investigation of B-Si defects properties in crystalline silicon, always upholding tight coupling and feedback among them. Combining tight-binding (TB) simulations and first-principles calculations we are able to locate the ground-state structures of neutral B-Si complexes with a limited computer cost, obtaining accurate formation and binding energies as a function of cluster size and composition. The TB simulations serve as scouts selecting the structures to be analyzed in depth via first-principles calculations: the portion of the configuration space to be explored with the more computer demanding *ab initio* techniques is in fact strongly reduced. Furthermore, the B-Si clusters are characterized in terms of their electronic struc-

0163-1829/2004/69(12)/125205(7)/$22.50 ©2004 The American Physical Society

tures to provide insight into the attribution of extrinsic levels to particular clusters arrangements. We restrict so far our *ab initio* study to the neutral B clusters, ignoring the possible structures associated to charged structures. Our idea is to identify structural fingerprints in the electronic properties of the clusters. A clear-cut attribution of electronic features under neutrality conditions can be very helpful in an analysis of the experimental data. Particularly, we focus our attention on aspects in the electronic density of states (DOS) related to interstitialcy and chemical nature of the aggregating atoms. As already pointed out, this kind of analysis is still missing in the literature.

The paper is organized as follows. In the following section we describe the computational methods we have used and we present the results on cluster geometries and energetics. In Sec. III the characteristics of the electronic structures of B_nI_m clusters are presented, through the analysis of the calculated electronic density of states.

II. CLUSTERS GEOMETRIES AND ENERGETICS

Our results have been obtained within a density-functional derived tight-binding (DFTB) (Ref. 7) scheme and they have been further analyzed by means of density-functional theory (DFT) calculations.

DFTB is a tight-binding model that explicitly incorporates the nonorthogonality of the basis set, which makes it more transferable. Furthermore, it is constructed from density-functional theory calculations via a series of well-defined approximations. These characteristics allow considerable savings in the computational effort with respect to full *ab initio* approaches, while still achieving remarkable accuracy in the calculations. Details of the DFTB parametrization for Si-B interactions are described in our previous paper,[8] where the DFTB method has been applied to the investigation of B atomic diffusion in crystalline Si.

For each B_nI_m cluster composition considered here (i.e., for each number n of B and m of interstitial atoms in the complex), we construct at first many possible structural candidates by educated guesses. We relax with DFTB the atomic positions in a $3\times3\times3$ replica of the conventional cubic cell, in order to find DFTB local energy minima and to extract the relevant B_nI_m geometries. In this way, we are able to perform a large number of preliminary structural relaxations. A restricted number of DFTB B_nI_m local minima are then used as input of first-principles calculations performed within DFT and using the Vienna *ab initio* simulation package (VASP).[9] The geometries obtained by the DFTB investigations are in fact further relaxed with the VASP code in a smaller $2\times2\times2$ supercell, until the atomic forces are $\leqslant 0.01$ eV/Å. Our investigation has been restricted to neutral clusters (i.e., no electronically charged). In order to converge all properties of relevance, we use a cut-off of 207 eV for the plane-wave expansion and a Monkhorst-Pack $4\times4\times4$ grid for the **k**-space summation. Ultrasoft pseudopotentials[10] describe the electron-ion interactions. We perform our calculations within both the generalized gradient approximation (GGA), in the Perdew-Wang formulation,[11] and the local-density approximation (LDA).[12] Our discussion is based on the GGA results, but comparisons with the LDA ones are present. With this choice of the cutoff parameters, we calculate the cluster binding energies as well as their electronic density of states.

TABLE I. Binding energies E_b (in eV) for the B_nI_m ground-state structures. Our DFTB and *ab initio* GGA and LDA results are reported in first, second, and third columns, respectively. Last two columns show the values published in Refs. 4 and 5.

	DFTB	GGA	LDA	GGA (Ref. 4)	LDA (Refs. 4 and 5)
B_2I_0	0.07	−0.78		−0.9	−0.9/−1.38
B_3I_0	−0.11	−1.20		−2.2	−2.3/−1.54
B_4I_0	−0.27	−1.85			
B_1I_1	0.43	1.15	0.91	0.5	0.4/0.79
B_2I_1	2.97	3.03	2.13	2.0	**1.2/2.12**
B_3I_1	4.22	4.14	2.87	3.0	2.2/**2.72**
B_4I_1	4.52	4.32		2.1	1.3
B_1I_2	3.23	2.74		2.5	2.3/2.2
B_2I_2	5.14	4.5		3.0	2.4/3.2
B_3I_2	6.72	5.58		**4.1**	**2.6**/4.4
B_4I_2	8.83	7.15		**5.5**	**4.3**/4.8
B_5I_2	9.5	7.67			

The binding energy E_b of a B_nI_m complex is defined here as the energy needed to split the cluster into n isolated neutral substitutional B_s atoms and m neutral Si self-interstitials. Since the ground state of the latter is the split $\langle 110\rangle$ dumbbell (X), the binding energy reads

$$E_b[B_nI_m]=\{E[B_nI_m]-N_{Si}\mu_{Si}-N_B\mu_B\}-m\cdot E_f[X], \tag{1}$$

where the quantity in brackets is the formation energy E_f of the B_nI_m defect, calculated from the total energy value $E[B_nI_m]$, the number N_{Si} (N_B) of Si (B) atoms in the supercell and the relative chemical potential μ_{Si} (μ_B). In the present work, we take μ_{Si} as the total energy per atom of bulk Si. Also, we consider the formation energy of neutral substitutional boron as the reference energy for formation energies of all other defects containing B atoms.

In Table I we report the binding energies of the B_nI_m ground-state structures, as calculated from Eq. (1). In order to compare the binding energy pictures of the B-I clustering obtained in the semiempirical and the *ab initio* frameworks, we list the DFTB values in first column and the DFT-GGA and DFT-LDA in second and third column's, respectively. Here we observe that not all values in Table I can be directly compared, since, as we will discuss in more details in the following, in few cases the DFTB ground-state structures differ from the GGA/LDA ones. Nevertheless, some arguments on the cluster energetics can be discussed from the table.

We note from Table I that DFTB binding energies differ from DFT values, with the difference between DFTB and LDA being more pronounced than with GGA values. The discrepancy between DFTB and DFT values is more evident in the case of $m=2$, where it increases with n at fixed m. This points out to a DFTB overestimation of B-B and B-SiI bond strengths. These features can be seen in Fig. 1, where

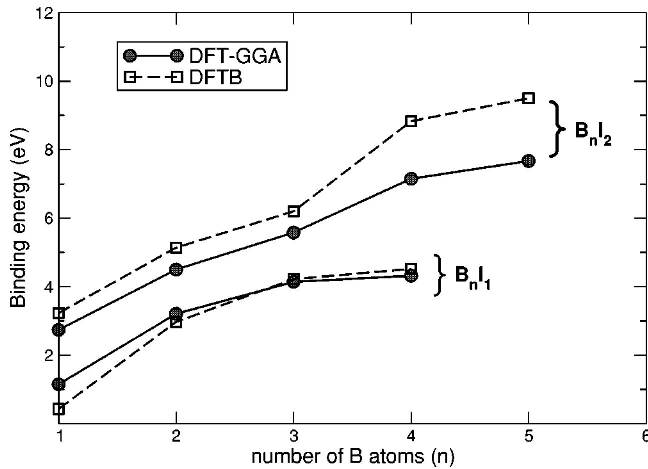

FIG. 1. DFTB and DFT-GGA values of binding energy for B_nI_1 and B_nI_2 clusters, as a function of the number of B atoms.

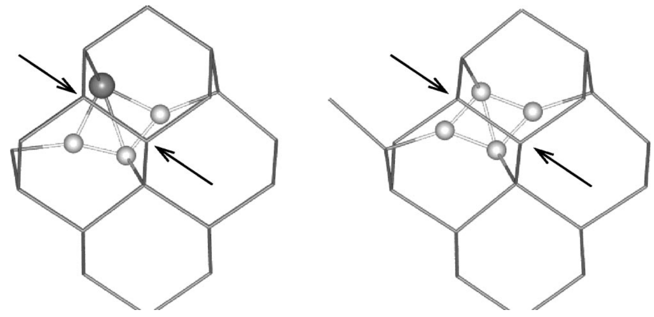

FIG. 2. Ground-state structures for B_3I_2 (left) and B_4I_2 (right). The arrows point to the two lattice sites where no Si atom is present. The four atoms forming the clusters are shown with spheres over the host silicon lattice (sticks): Si-I with black spheres and large atomic radius, and B atoms as white spheres.

we plot DFTB and GGA binding-energy values, for a better visual representation. It is also clear from the picture that, although the energetics of B_nI_m clusters obtained in the tight-binding model and from first-principles calculations differs in absolute values, some general characteristics do not. By this we mean that, within all methodological frameworks it turns out that (i) pure substitutional B_nI_0 clusters are unstable, showing a negative binding energy; (ii) E_b at fixed m increases as a function of the number n of B atoms; (iii) E_b levels up at $n=3$ for $m=1$, and $n=4$ for $m=2$.

Both LDA and GGA values follow the general trends listed above. The two exchange-correlation functionals give also the same B_nI_m minimum energy structures. However, LDA binding energies are in general lower than GGA values, by $\simeq 1$ eV. This is also consistent with the results on GGA and LDA binding energies obtained by Liu and co-workers,[4] that we report in last two columns of Table I.

In order to better understand these features of the B-I clusters energetics, let us first briefly present the GGA ground-state geometries for the different compositions. We proceed by discussing structures with a fixed number m of interstitials and increasing number n of B atoms.

As reported above, we find that pure substitutional clusters ($m=0$) have negative binding energy if the number of B atoms involved is $n \geqslant 2$. This is actually expected from geometrical considerations, since B-B distances in full substitutional clusters are strained to match the Si-Si nearest neighbor distance $d=2.36$ Å, so that adding B atoms in substitutional lattice sites becomes unfavorable.

As for the configurations of B_nI_1, LDA, and GGA equilibrium geometries for neutral clusters coincide with the geometries reported in the work of Liu *et al.*,[4] which are however obtained for negatively charged complexes. In particular, we obtain a substitutional B_s with a SiI in a nearby tetrahedral site for B_1I_1, a B-B $\langle 100 \rangle$-dumbbell for B_2I_1 and the bond-center interstitial B_{BC} between two nearest-neighbor B_s atoms for B_3I_1. In the B_4I_1 and B_5I_1 clusters, further B_s atoms are added to the B_3I_1 structure. As already mentioned in Ref. 8, the DFTB calculations give a different geometry for the B_1I_1 with respect to *ab initio* results and we refer the reader to that paper for a more accurate discussion. Instead, we point out here that for the other B_nI_1 cases the DFTB and DFT geometries coincide.

We have already pointed out that the B_nI_1 binding energy increases with the number of B atoms and it levels up at $n=3$ in all frameworks. From there on, in fact, there is no further binding-energy gain in adding B atoms while keeping $m=1$. This can be understood from the same arguments as in the case of pure substitutional B clusters: the smaller volume of the B atoms and their tendency to be threefold coordinated makes it less favorable to form B-B bonds between substitutional sites.

We then turn to the B_nI_2 ground-state structures starting, for reasons that will be clear in the following, from $n=3$. As it can be noticed in Fig. 2, the B_3I_2 geometry is similar to that of the B_4I_2 complex: it is a planar structure, with the four atoms of the defect lying on the (110) plane. The B_4I_2 structure originates from placing two $\langle 100 \rangle$ B-B dimers in adjacent lattice sites. In B_nI_2 complexes with $n \geqslant 4$, substitutional B atoms are added to the B_4I_2 structure. Here also, the increase in binding energies levels up at $n=4$, both in DFTB and DFT calculations. We can thus indicate an upper ratio of B to interstitials atoms as $\simeq 3:1$.

As for the B_1I_2 and B_2I_2, DFT-GGA structures are different from the DFTB ones. In particular, we show in Fig. 3 the case of B_2I_2, with the ground-state DFTB and DFT-GGA configurations in the upper-left and lower-right panels, respectively. The DFT-GGA configuration has been obtained after a VASP relaxation of the metastable DFTB geometry that is showed in the lower-left panel. This gives us the opportunity to discuss some features of DFTB and DFT relaxations.

According to the calculation strategy described above, we extract from the DFTB calculations four relaxed structures with formation energy differences being within a range of $\simeq 0.5$ eV. The ground-state DFTB geometry [Fig. 3(a)] looks like it is made up of a BB-dimer located in the middle of the hexagonal ring of the silicon lattice. We further relax the four DFTB structures with VASP, and we obtain a different energy order among them, and slightly different ionic relaxations. We mention here that a typical VASP relaxation of a DFTB geometry took $\leqslant 10$ ionics iterations, resulting in

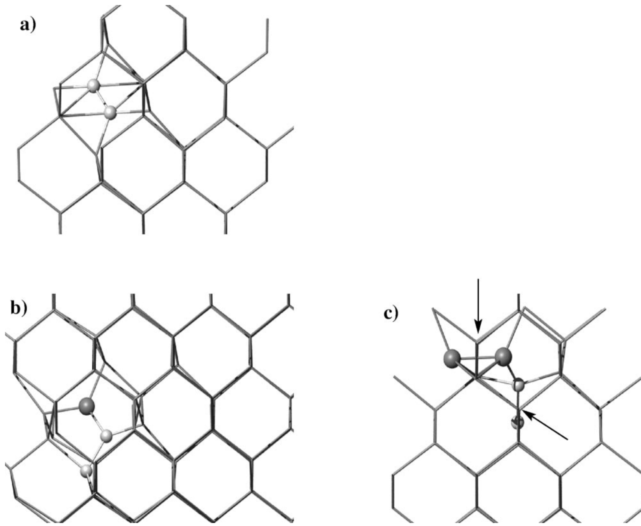

FIG. 3. DFTB (left) and VASP (right) relaxed structures for B_2I_2. Selected atoms are shown with spheres over the host silicon lattice (sticks): all B atoms in the cell (white spheres) and the Si-I atoms (black spheres, large atomic radius). The arrows point to the lattice sites where no silicon atom is present.

a gain in computational time with respect to a full *ab initio* relaxation procedure starting from a completely unrelaxed structure. The DFT relaxation brought the ground-state DFTB structure into a more symmetrical one, made up from two mixed Si-B dumbbell, oriented along the $\langle 110 \rangle$ and the $\langle 100 \rangle$ directions. Moreover, another DFTB structure [Fig. 3(b)], further relaxed with VASP, resulted to be almost degenerate in energy with the previous one (both in LDA and in GGA): it is made up from the two stable single-specie interstitials, the Si-$\langle 110 \rangle$ and B-$\langle 100 \rangle$ dumbbells [Fig. 3(c)]. These two VASP structures have a planar geometry. A third one, containing triangular shapes, is higher in energy (by 0.36 eV). It corresponds to the complex found by Liu *et al.* In general, the structures with $m=2$ differ from the ones published by Liu *et al.*,[4] since all their B_nI_2 structures contain triangles forming the surface of icosahedra and are not planar. Since that work was carried out entirely through *ab initio* calculations, computationally more demanding, we believe that the discrepancy might be due to a less accurate sampling of the configurational space performed by Liu *et al.* The DFTB calculations has given us access to a larger portion of the B-I complex configuration space.

We also mention here that the DFT-GGA B_1I_2 ground state has a planar geometry, consisting in two interstitial atoms forming a Si-B $\langle 110 \rangle$ dimer located in the middle of the silicon hexagonal rings.

Let us now turn briefly to a comparison of our binding-energy values with those reported in previous works. Since Liu and co-workers[4] considered in their investigations all possible charge states of the clusters, a comparison can be consistently made only for the cases where the neutral states is the lowest energy one. In Table I, we indicate in bold the binding energies of Ref. 4 where an exact correspondence with our structures exists, both as what regards geometries and charge states. The values of E_b are calculated with different choices of the reference energies. Our values are in fact always referred to the neutral isolated defects B_s and SiI-X. On the other hand, both LDA and GGA binding energies of Ref. 4 are calculated with respect to isolated B_s^- and neutral SiI-X. In all cases where a consistent comparison can be made, we obtain larger values of binding energies. This is correct, since the ground state of a substitutional B atom is the negatively charged B_s^-, at all Fermi-level positions.[13] If two choices of the chemical potential are made in Eq. (1) the binding-energy difference ΔE_b is in fact equal to $n * \Delta \mu_B$.[14] From a separate calculation of GGA B_s^-, we thus estimate $\Delta E_b \simeq 0.4\ n$ eV, which is consistent with values reported in Table I. The reference states of Ref. 5 are instead the charged defects B_s^- and the self-interstitial SiI-Td^{++}, the double charged tetrahedral defect. Here, a comparison is also made more difficult by the fact that the cluster geometries are not reported, and we cannot be sure of neutral ground-state structure correspondence.

In conclusions, although the calculated DFTB binding energies are larger than the first-principles values, the DFTB method is shown to be overall quite accurate in predicting the geometries of B-I clusters and the characteristics of the B-SiI bonds. Cluster geometries having the same composition but different rearrangements of Si—B, Si—Si, and B—B bonds differ in energy by few tenths of eV. This energy difference might not be within the accuracy of the DFTB method, resulting in slightly different order among stable and metastable structures with respect to *ab initio* results. Nevertheless, the overall trends of the cluster energetics are accurately predicted by DFTB. At least to our knowledge, this represents a great improvement with respect to previous tight-binding investigation of the B-Si clustering process.[15]

III. DENSITY OF STATES OF NEUTRAL CLUSTERS

The electronic densities of states are calculated with a Monkhorst-Pack $5 \times 5 \times 5$ **k**-points sampling, using the VASP package. Only selected structures have been reported here. The first step is the calculation of the DOS for the crystalline Si matrix. The results are reported in Fig. 4(a). Note that all the DOS's presented in this section are shifted according to the respective calculated Fermi energy (E_F). We focus our analysis on some characteristics of the DOS, that we list here: presence of gap states; their location with respect to E_F; presence of other localized states.

A known failure of density-functional theory calculations is the determination of the silicon band gap. We decide not to use any band-gap corrections and we consistently obtain, at the theoretical GGA lattice constant, a GGA band gap of $E_g = 0.69$ eV, smaller than the experimental gap of 1.13 eV, but in accordance with other theoretical studies.[16] Note that the LDA gap is $E_g = 0.55$ eV.

The other two panels of Fig. 4 collect the DOS for the Si crystal with two kind of self-interstitial defects: (b) a dumbbell, Si-X, and (c) a tetrahedral Si atom, Si_{Td}. In the latter case there is a shift of the calculated Fermi level towards the conduction band, which can be interpreted as an effect of the

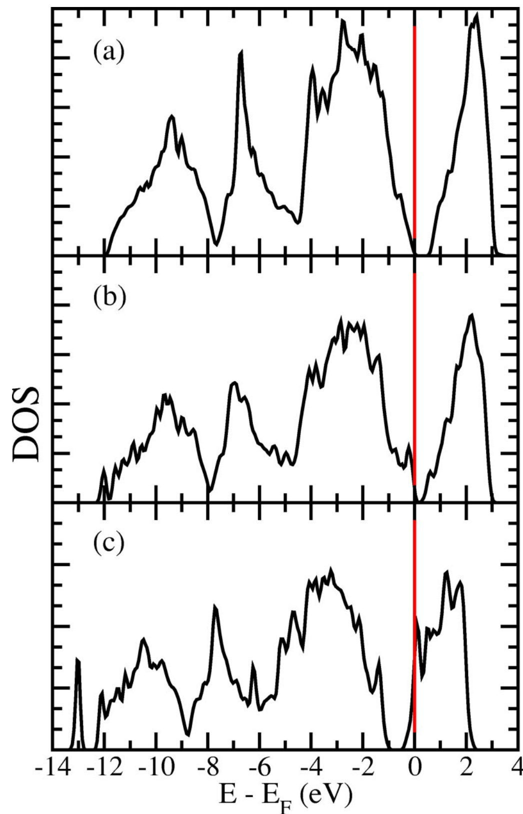

FIG. 4. Density of states of (a) silicon bulk, (b) silicon interstitial in the dumbbell, and (c) tetrahedral. The zero of the energy scale corresponds to the calculated Fermi level associated to the structure. This procedure has been adopted for all the other DOS's.

over-coordination of the Si atoms surrounding the tetrahedral defect. Moreover, at an energy of about -13 eV a clearly localized peak appears. This feature is absent in the DOS related to the perfect crystal, but it can be recognized also in the panel (b) of Fig. 4, closer to the bottom of the valence band than in the tetrahedral case. The analysis of the localized-DOS identifies these peaks to the structure around the defects, with a stronger character for the tetrahedral one. These peaks should result from the A_1-T_2 splitting induced at the bottom of the valence band by the silicon interstitial, as already discussed in literature.[17] A final remark is on the position of the Fermi level in the DOS of Fig. 4(b): it corresponds to a localized structure slightly above the top of the valence band. This feature is present in the DOS of panel (c), but corresponds to a fully occupied state. This difference can be ascribed to the different character of the localization region of the state: both peaks are attributed to the region around the defects, but the dumbbell is over coordinated, while the tetrahedral has nearly a bulk configuration.

Figure 5(a) shows the calculated DOS for a B atom in a substitutional site (B_1I_0), that is, the ideal doping position. As expected, the Fermi level cuts the DOS just above the top of the valence band, in accordance with the textbook description of a *p* doping. Interestingly, there are no features below the valence band. This indicates that the presence of the states observed in Figs. 4(b) and 4(c) might be traced back to the interstitial character of atoms composing the aggregates, that is, to their spatial departure from a crystalline site. We will discuss further this issue.

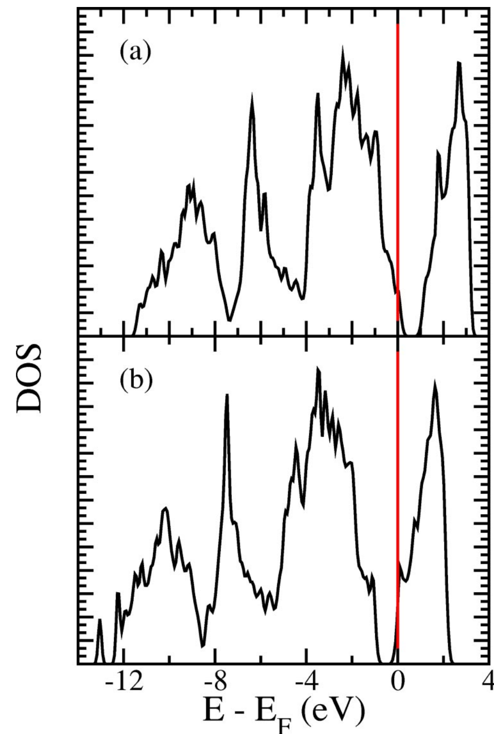

FIG. 5. Density of states of a crystalline Si matrix with (*a*) a single B atom in a substitutional site (B_1I_0) and (*b*) a B_1I_1 defect (B_s+Si_{Td}).

In Fig. 5(b) we report the DOS for the ground-state B_1I_1 defect (B_s+Si_{Td}). We want in fact to extract from the plotted DOS the features that can be ascribed to the presence of B substituting a silicon atom or to the presence of both (B in a lattice site and Si in a tetrahedral position). All the features already pinpointed from the analysis of the panels collected in Fig. 4 are easily identified. The peak below the valence-band bottom is still present. The main difference is the relative intensity of the above features. For example, the ratio between the peak at $\simeq 13$ eV and a pronounced bulk structure (peak at $\simeq 7.4$ eV) changes from 0.64 (Si_{Td}) to 0.18 ($B_1I_1:B_s+Si_{Td}$). The intensity seems to be related to the chemical species involved in the bonding, while the position is determined by the interstitial character of one of the components. Further comparisons should help in putting on surer foots this physical picture. Therefore, we monitor the electronic structure evolution during atomic relaxation processes of the system containing a B atom toward the $B_1I_1:B_s+Si_{Td}$ compound.

Four snapshots of the relaxing configurations are collected in Fig. 6, while in Fig. 7 the corresponding DOS's are shown. The initial configuration [panel (a)] corresponds to the B atom in a slightly interstitial position and the corresponding DOS exhibits a structure close to the bottom of the valence band. We note also that in the four snapshots in Fig. 6 the symmetry of the defect configuration changes from C_{1h} to C_{3v}. Increasing the interstitialcy of the Si atom (with a consequent lowering of the intersticial character of the B

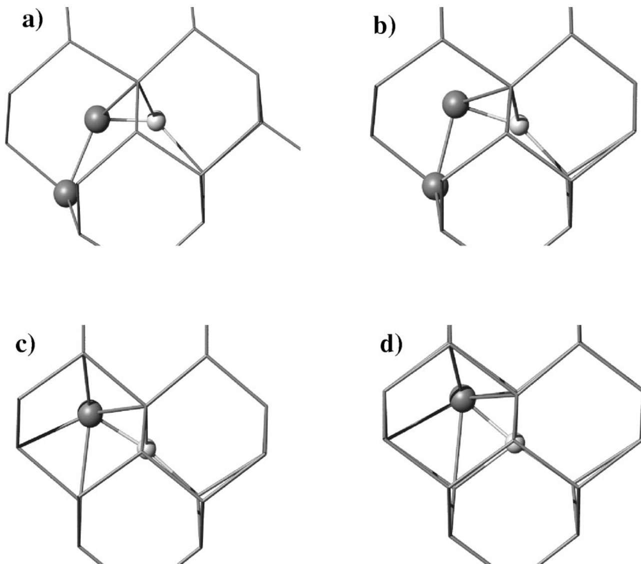

FIG. 6. Snapshots of the relaxation of the system containing a B atom toward the B_s+Si_{Td} compounds. The panel (*a*) denotes the starting position, the panel (*d*) a configuration closer to B_s+Si_{Td}.

position), the peak is pushed out from the valence band [panel (b)]. In the panels (c) and (d) the peak has assumed nearly its final position. It is interesting to note the oscillating behavior of the intensity: stronger in panels (b) and (c) [and also in Fig. 5(b)] than in panel (d). This apparent discrepancy is probably due to the interplay of two different degrees of intersticialcy (the one of B and the one of Si) and the electronic properties of the two species. It is practically impossible to identify from these sets of DOS's the two contributions to the effect. Thus, the criterion above proposed that connects the intensity to the chemical nature of the components and the energy position to the interstitialcy degree should be reformulated.

We have also examined other DOS's, and a further indication of the subtle interplay between the two aspects is extracted from the analysis of Fig. 8, where the DOS's for the clusters (a) B_2I_1 and (b) B_3I_1 are collected. These aggregates are characterized by the presence of interstitial B atoms without any interstitial Si. The structure below the bottom of the valence band is absent in both DOS's, pointing out the relatively *small* perturbing effect of these particular B-cluster configurations on the low-energy part of the electronic spectrum of the system. On the other hand, the localized peak is observed in both panels of Fig. 9 at $\simeq -12$ eV, i.e., both

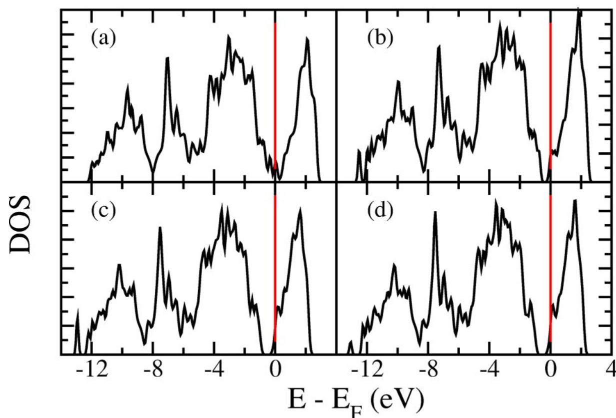

FIG. 7. DOS's corresponding to the configurations collected in Fig. 6.

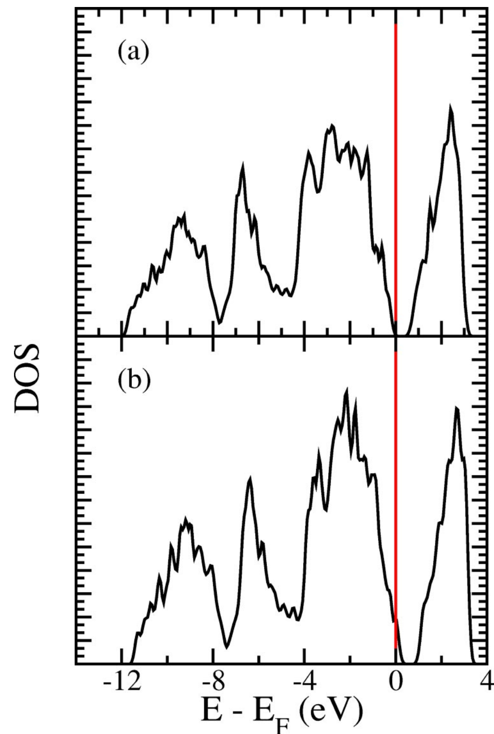

FIG. 8. Density of states of (a) B_2I_1 and (b) B_3I_1.

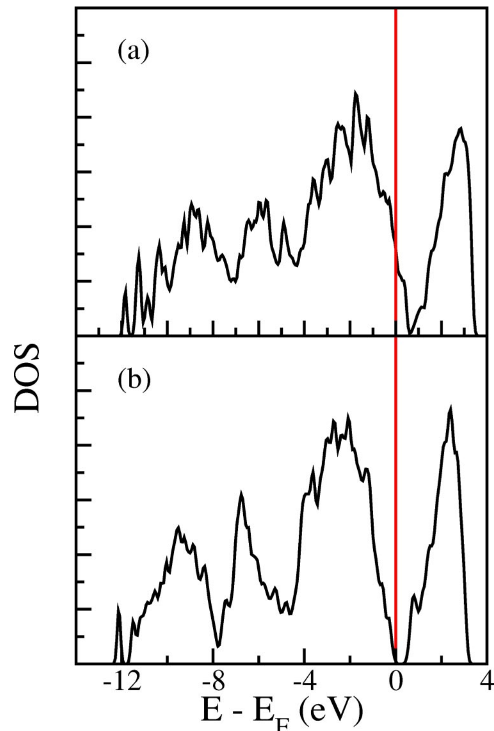

FIG. 9. DOS of (a) B_3I_2 and (b) B_4I_2.

when interstitial atoms of different chemical species are present [B_3I_2, in panel (a)], and when all interstitial are B atoms [B_4I_2, in panel (b)].

Thus, the symmetry lowering due to the presence of interstitial atoms induces the *A-T* splitting of the electronic states at the lower valence-band edge, while the relative strengths of B-Si, Si-Si, B-B interactions shifts these electronic states upper or lower in energy (i.e., inside or outside the valence-band core). We conclude that it is not possible to ascribe in a general and conclusive way the presence of electronic states at $\simeq -12$ eV to the cluster compositions.

A final remark concerns the electrical activity of the microaggregates, connected to the presence of states in the gap of the system. Some configurations fulfill this requirement and can contribute to the doping-induced carrier flow, in complete analogy with the behavior of a single substitutional B atom. This is the case of B_3I_1 [Fig. 8(b)] and of B_3I_2 [Fig. 9(a)], for example. However, it should be stressed that the electrical activity of such a cluster involves several B atoms, each of them independently located in a substitutional site producing the same contribution to the electrical activity than the aggregate. Thus, there is a clear decrease in the efficiency of the doping process, as far as clusters are formed. With larger clusters the ratio *B atoms/electrical activity* even worsens, although gap states may occur. An interesting point is related to the DOS's of B_2I_1 (upper panel of Fig. 8) and B_4I_2 (lower panel of Fig. 9) which show no defect states in the fundamental gap. The configuration topology of these clusters is particularly favorable for B atoms, since they result to be three-fold coordinated, with a B-B distance of ~ 1.63 Å. This explains the absence of states in the band gap.

IV. CONCLUSIONS

In this work we have combined the information extracted from semiempirical large-size simulation runs based on the DFTB approach with *ab initio* calculations, exploring in this way a very large portion of the configuration space of B aggregates in Si crystals. The comparison between the two sets of calculations validates several DFTB predictions and enables the identification of structures not picked out by previous first-principles studies. Although we have restricted our investigation to neutral clusters, the picture extracted from our calculations can provide insights in general mechanisms of clustering, enabling the identification of specific fingerprints. According to our results pure substitutional B_nI_0 clusters are energetically unfavorable with negative binding energies. Interstitial companions are necessary to stabilize the aggregates, and the binding-energy increases at a fixed number of interstitials by addition of B atoms to the structure. The interstitialcy degree of the cluster and the chemical nature of its components interweave subtly in determining localized features in the DOS's, as pointed out by our analysis of the electronic properties. However, it is not possible to yield clear-cut criteria to quantify the single contributions.

ACKNOWLEDGMENTS

We acknowledge financial support by MIUR under P.R.I.N.-2002 project *Dopant diffusion and clustering in crystalline silicon in the high concentration, high strain, and codoping regime*. We also acknowledge computational support by INFM under the Parallel Computing Initiative.

*Electronic address: paola.alippi@imm.cnr.it

[1] S.C. Jain, W. Schoenmaker, R. Lindsay, P.A. Stolk, S. Decoutere, M. Willander, and H.E. Maes, J. Appl. Phys. **91**, 8919 (2002).

[2] P.A. Stolk, H.-J. Gossmann, D.J. Eaglesham, D.C. Jacobson, and J.M. Poate, Appl. Phys. Lett. **66**, 568 (1995); T.E. Haynes, D.J. Eaglesham, P.A. Stolk, H.-J. Gossmann, D.C. Jacobson, and J.M. Poate, *ibid.* **69**, 1376 (1996).

[3] L. Pelaz, G.H. Gilmer, H.-J. Gossmann, C.S. Rafferty, M. Jaraiz, and J. Barbolla, Appl. Phys. Lett. **74**, 3657 (1999).

[4] X.-Y. Liu, W. Windl, and M.P. Masquelier, Appl. Phys. Lett. **77**, 2018 (2000).

[5] T.J. Lenosky, B. Sadigh, S.K. Theiss, M.-J. Caturla, and Th.D. de la Rubia, Appl. Phys. Lett. **77**, 1834 (2000).

[6] B.P. Uberuaga, G. Henkelman, H. Jonsson, S.T. Dunham, W. Windl, and R. Stumpf, Phys. Status Solidi B **233**, 24 (2002).

[7] D. Porezag, Th. Frauenheim, Th. Koeheler, G. Seifert, and R. Kaschner, Phys. Rev. B **51**, 12 947 (1995); M. Elstner, D. Porezag, G. Jungnickel, J. Elsner, M. Haugk, Th. Frauenheim, S. Suhai, and G. Seifert, *ibid.* **58**, 7260 (1998).

[8] P. Alippi, L. Colombo, P. Ruggerone, A. Sieck, G. Seifert, and Th. Frauenheim, Phys. Rev. B **64**, 075207 (2001).

[9] G. Kresse and J. Hafner, Phys. Rev. B **47**, 558 (1993); **49**, 14251 (1994); G. Kresse and J. Furthmüller, Comput. Mater. Sci. **6**, 15 (1996); Phys. Rev. B **54**, 11 169 (1996).

[10] D. Vanderbilt, Phys. Rev. B **40**, 7892 (1990).

[11] J. P. Perdew, in *Electronic Structure of Solids '91*, edited by P. Ziesche and H. Eschrig (Akademie-Verlag, Berlin, 1991), p. 11.

[12] D. Ceperley and B.J. Alder, Phys. Rev. Lett. **45**, 566 (1980); J.P. Perdew and A. Zunger, Phys. Rev. B **23**, 5048 (1981).

[13] M. Hakala, M.J. Puska, and R. Nieminen, Phys. Rev. B **61**, 8155 (2000).

[14] The difference in B_nI_m binding energies due to different choice of reference energies is $\Delta E_b = n*\Delta\mu_B + m\Delta E_f[\mathrm{X}]$.

[15] W. Luo and P. Clancy, J. Appl. Phys. **89**, 1596 (2001).

[16] W. Windl, M.M. Bunea, R. Stumpf, S.T. Dunham, and M.P. Masquelier, Phys. Rev. Lett. **83**, 4345 (1999).

[17] Y. Bar-Yam and D. Joannopoulus, Phys. Rev. B **30**, 1844 (1984).